

Entanglement Suppression and Emergent Symmetries of Strong Interactions

Silas R. Beane,¹ David B. Kaplan,² Natalie Klco,^{1,2} and Martin J. Savage²

¹*Department of Physics, University of Washington, Seattle, WA 98195-1560, USA*

²*Institute for Nuclear Theory, University of Washington, Seattle, WA 98195-1550, USA*

(Dated: March 17, 2022 - 17:51)

Entanglement suppression in the strong interaction S -matrix is shown to be correlated with approximate spin-flavor symmetries that are observed in low-energy baryon interactions, the Wigner $SU(4)$ symmetry for two flavors and an $SU(16)$ symmetry for three flavors. We conjecture that dynamical entanglement suppression is a property of the strong interactions in the infrared, giving rise to these emergent symmetries and providing powerful constraints on the nature of nuclear and hypernuclear forces in dense matter.

Understanding approximate global symmetries in the strong interactions has played an important historical role in the development of the theory of Quantum Chromodynamics (QCD). Baryon number symmetry arises in QCD because it is impossible to include a marginal or relevant interaction consistent with Lorentz and gauge symmetry which violates baryon number, while the axial and vector flavor symmetries are understood to be due to the small ratio of quark masses (and their differences) to the QCD scale. The approximate low-energy $SU(2n_f)$ spin-flavor symmetry for $n_f = 2, 3$ flavors which relates spin-1/2 and spin-3/2 baryons can be understood as arising at leading order (LO) in the large- N_c expansion, where N_c is the number of colors [1, 2]. In low-energy nuclear physics, a different spin-flavor symmetry is observed in the structure of light-nuclei and their β -decay rates, namely Wigner's $SU(4)$ symmetry, where the two spin states of the two nucleons transform as the 4-dimensional fundamental representation [3–5]. It has been shown that this symmetry also arises from the large- N_c expansion at energies below the Δ mass [6–8]. The agreement of large- N_c predictions with nuclear phenomenology has been extended to higher-order interactions [9–12], three-nucleon systems [13–15], and to studies of hadronic parity violation [16–18]. Recently, however, lattice QCD computations for $n_f = 3$ have revealed an emergent $SU(16)$ symmetry in low-energy interactions of the baryon octet—analogous to Wigner's $SU(4)$, but with the two spin states of the eight baryons transforming as the 16-dimensional representation of $SU(16)$ [19]. This low energy symmetry has been lacking an explanation from QCD. In this Letter, we show that both Wigner's $SU(4)$ symmetry for $n_f = 2$ and $SU(16)$ for $n_f = 3$ correspond to fixed lines of minimal quantum entanglement in the S -matrix for baryon-baryon scattering, and we propose entanglement suppression to be a dynamical property of QCD and the origin of these emergent symmetries ¹.

Of the many features of quantum mechanics and quantum field theory (QFT) that dictate the behavior of subatomic particles, entanglement and its associated non-locality are perhaps the most striking in their contrast to everyday experience. The degree to which a system is entangled, or its deviation from tensor-product structure, provides a measure of how “non-classical” it is. The importance of entanglement as a feature of quantum theory has been known since the work of Einstein, Podolsky and Rosen [21] and later pioneering papers [22–24], and has become a core ingredient in quantum information science, communication and perhaps in understanding the very fabric of spacetime [25–27]. Despite this long history, the implications of entanglement in QFTs, e.g., Refs. [28–39], and in particular for experimental observables in high-energy and heavy-ion collisions are only now starting to be explored [20, 40–49]. Here we study the role of entanglement in low-energy nuclear interactions.

In general, a low-energy scattering event can entangle position, spin, and flavor quantum numbers, and it is therefore natural to assign an entanglement power to the S -matrix for nucleon-nucleon scattering. We choose to define the entanglement power of the S -matrix in a two-particle spin space [50, 51], noting that this choice is not unique and that others will be explored elsewhere [52]. This is determined by the action of the S -matrix on an incoming two-particle tensor product state with randomly-oriented spins, $|\psi_{\text{in}}\rangle = \hat{R}(\Omega_1)|\uparrow\rangle_1 \otimes \hat{R}(\Omega_2)|\uparrow\rangle_2$, where $\hat{R}(\Omega_j)$ is the rotation operator acting in the j^{th} spin- $\frac{1}{2}$ space, and all other quantum numbers associated with the states have been suppressed. For low-energy processes, this random spin pair projects onto the two states with total spin $S = 0, 1$, and associated phase shifts $\delta_{0,1}$, in the 1S_0 and 3S_1 channels, respectively, with projections onto higher angular momentum states suppressed by powers of the nucleon momenta. The entanglement power, \mathcal{E} , of the S -matrix, \hat{S} , is defined as

$$\mathcal{E}(\hat{S}) = 1 - \int \frac{d\Omega_1}{4\pi} \frac{d\Omega_2}{4\pi} \text{Tr}_1 [\hat{\rho}_1^2] , \quad (1)$$

where $\hat{\rho}_1 = \text{Tr}_2 [\hat{\rho}_{12}]$ is the reduced density matrix for particle 1 of the two-particle density matrix $\hat{\rho}_{12} =$

¹ A principle of *maximum* entanglement has been previously proposed to constrain quantum electrodynamics in Ref. [20].

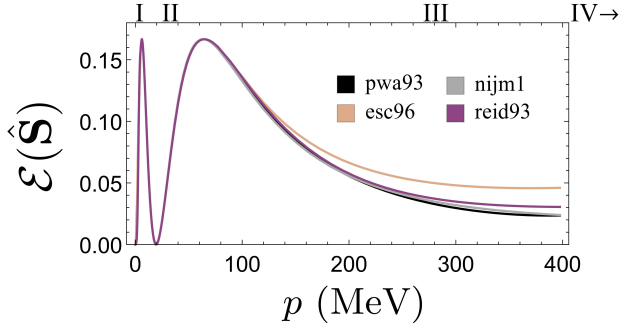


FIG. 1. The entanglement power, $\mathcal{E}(\hat{\mathbf{S}})$, of the S -matrix as a function of p , the center-of-mass nucleon momentum. The 1S_0 and 3S_1 phase shifts used to calculate $\mathcal{E}(\hat{\mathbf{S}})$ were taken from four different models [53–57] to provide a naïve estimate of systematic uncertainties. Data for this figure may be found in Table II in the supplemental material.

$|\psi_{\text{out}}\rangle\langle\psi_{\text{out}}|$ with $|\psi_{\text{out}}\rangle = \hat{\mathbf{S}}|\psi_{\text{in}}\rangle$. By describing the average action of $\hat{\mathbf{S}}$ to transition a tensor-product state to an entangled state, the entanglement power expresses a state-independent entanglement measure that vanishes when $|\psi_{\text{out}}\rangle$ remains a tensor product state for any $|\psi_{\text{in}}\rangle$.

Following the analysis of Ref. [20], we consider the spin-space entanglement of two distinguishable particles, the proton and neutron for $n_f = 2$ QCD. Neglecting the small tensor-force-induced mixing of the 3S_1 channel with the 3D_1 channel, the S -matrix for low-energy scattering below inelastic threshold in these sectors can be decomposed as

$$\hat{\mathbf{S}} = \frac{1}{4} (3e^{i2\delta_1} + e^{i2\delta_0}) \hat{\mathbf{1}} + \frac{1}{4} (e^{i2\delta_1} - e^{i2\delta_0}) \hat{\boldsymbol{\sigma}} \cdot \hat{\boldsymbol{\sigma}}, \quad (2)$$

where $\hat{\mathbf{1}} = \hat{\mathcal{I}}_2 \otimes \hat{\mathcal{I}}_2$ and $\hat{\boldsymbol{\sigma}} \cdot \hat{\boldsymbol{\sigma}} = \sum_{\alpha=1}^3 \hat{\boldsymbol{\sigma}}^\alpha \otimes \hat{\boldsymbol{\sigma}}^\alpha$. It follows that the entanglement power of $\hat{\mathbf{S}}$ is

$$\mathcal{E}(\hat{\mathbf{S}}) = \frac{1}{6} \sin^2(2(\delta_1 - \delta_0)), \quad (3)$$

which vanishes when $\delta_1 - \delta_0 = m\frac{\pi}{2}$ for any integer m . This includes the $SU(4)$ symmetric case $\delta_1 = \delta_0$ where the coefficient of $\hat{\boldsymbol{\sigma}} \cdot \hat{\boldsymbol{\sigma}}$ vanishes. Special fixed points where the entanglement power vanishes occur when the phase shifts both vanish, $\delta_1 = \delta_0 = 0$, or are both at unitarity, $\delta_1 = \delta_0 = \frac{\pi}{2}$, or when $\delta_1 = 0$, $\delta_0 = \frac{\pi}{2}$ or $\delta_1 = \frac{\pi}{2}$, $\delta_0 = 0$. The S -matrices at these fixed points with vanishing entanglement power are $\hat{\mathbf{S}} = \pm \hat{\mathbf{1}}$ and $\pm (\hat{\mathbf{1}} + \hat{\boldsymbol{\sigma}} \cdot \hat{\boldsymbol{\sigma}})/2$ ².

The entanglement power in nature is plotted in Fig. 1 as a function of the center-of-mass nucleon momentum, p , up to pion production threshold, making use of the 1S_0 and 3S_1 phase shifts derived from the analyses of

Refs. [53–56]. The four regions indicated are distinguished by the role of non-perturbative physics. Region I shows that entanglement power approaches zero in the limit $p \rightarrow 0$, as will be the case for any finite range interaction not at unitarity. At momenta around the scale of the inverse scattering lengths, region II, poles and resonances of $\hat{\mathbf{S}}$ produce highly-entangling interactions. This non-perturbative structure could be considered a source of ultra-low-momentum entanglement power; experimental evidence for this is expected to be found in the vanishing modification of np -scattering quantum correlations at 19.465(42) MeV where the phase shifts differ by $\pi/2$ and $|p\uparrow, n\downarrow\rangle$ scatters into $|p\downarrow, n\uparrow\rangle$. In region IV, where energies are of order the chiral symmetry breaking scale, the entangling interactions of quark and gluon degrees of freedom become prominent. It is region III that is the main focus of this paper—away from the far-infrared structure but with nucleons as fundamental degrees of freedom, the entanglement power is suppressed. Once relativistic corrections and 3S_1 - 3D_1 mixing—parametrically suppressed at low-energy—are included in Eq. (19), $\mathcal{E}(\hat{\mathbf{S}})$ is expected to remain suppressed but non-zero, indicating that the entanglement suppression in nature is only partial.

Much progress has been made in nuclear physics in recent years by considering low-energy effective field theories (EFTs), constrained by data from nucleon scattering. The $\delta_{0,1}$ phase shifts can be computed for energies below the pion mass, from the pionless EFT for nucleon-nucleon interactions. The leading interaction in the effective Lagrangian is

$$\mathcal{L}_{\text{LO}}^{n_f=2} = -\frac{1}{2} C_S (N^\dagger N)^2 - \frac{1}{2} C_T (N^\dagger \boldsymbol{\sigma} N) \cdot (N^\dagger \boldsymbol{\sigma} N), \quad (4)$$

where N represents both spin states of the proton and neutron fields. These interactions can be re-expressed as contact interactions in the 1S_0 and 3S_1 channels with couplings $\bar{C}_0 = (C_S - 3C_T)$ and $\bar{C}_1 = (C_S + C_T)$ respectively, where the two couplings are fit to reproduce the 1S_0 and 3S_1 scattering lengths. The \bar{C} coefficients both run with the renormalization group as described in Ref. [58, 59] with a stable IR fixed point at $\bar{C} = 0$, corresponding to free particles, and a nontrivial, unstable IR fixed point at $\bar{C} = C_*$ corresponding to a divergent scattering length and constant phase shift of $\delta = \pi/2$ (the “unitary” fixed point). At the four fixed points (described above), where $\{\bar{C}_0, \bar{C}_1\}$ take the values 0 or C_* , the theory has a conformal (“Schrödinger”) symmetry; there is also a fixed line of enhanced symmetry at $C_T = 0$, or equivalently $\bar{C}_0 = \bar{C}_1$, where the theory possesses the Wigner $SU(4)$ symmetry, as apparent from the form of Eq. (4) with $C_T = 0$. When fitting to the scattering lengths one finds $C_T \ll C_S \simeq C_*$, since scattering lengths are unnaturally large in both channels. Therefore, low-energy QCD has approximate $SU(4)$ symmetry and sits close to the $\{C_*, C_+\}$ conformal fixed point [60]. The emer-

² The S -matrices at the four fixed points realize a representation of the Klein four-group, $\mathbb{Z}_2 \otimes \mathbb{Z}_2$.

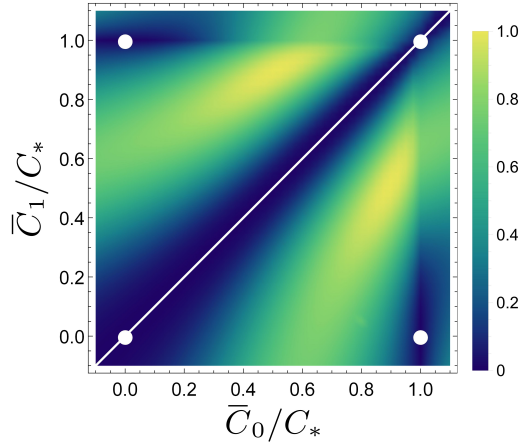


FIG. 2. Density plot of the entanglement power $\mathcal{E}(\hat{\mathbf{S}})$ of the S -matrix (see Eq. (20) of the supplemental material) integrated over center of mass momenta $0 \leq p \leq m_\pi/2$, versus the Lagrangian couplings \bar{C}_0/C_* and \bar{C}_1/C_* where C_* is the critical coupling for unitary scattering. The entanglement power vanishes at the four conformal fixed-points (white points), as well as the fixed line corresponding to Wigner $SU(4)$ symmetry (white diagonal).

gence of $SU(4)$ symmetry (but not necessarily conformal symmetry) follows from the large- N_c expansion where $C_T/C_S = O(1/N_c^2)$ [6].

The symmetry points of the EFT can be related to minimization of the entanglement power of the S -matrix. Fig. 2 shows a density plot of $\mathcal{E}(\hat{\mathbf{S}})$ as computed from Eq. (4) averaged over momenta $0 \leq p \leq m_\pi/2$, as a function of the couplings $\bar{C}_{0,1}$ renormalized at $\mu = m_\pi/2$ and rescaled by C_* . Superimposed in white are the four conformal fixed points, as well as the Wigner $SU(4)$ fixed line. The minima of the entanglement power of the S -matrix ($\mathcal{E}(\hat{\mathbf{S}}) = 0$) coincide with the points of enhanced symmetry in the EFT; the $SU(4)$ line corresponds to $\delta_0 = \delta_1$ for all momenta, while the conformal points off the $SU(4)$ line correspond to $|\delta_0 - \delta_1| = \pi/2$.

In the $n_f = 2$ case, the large- N_c expansion gives a similar expectation for $SU(4)$ symmetry as does a principle of entanglement suppression. However, an analogous equivalence does not hold for $n_f = 3$, as the large- N_c expansion predicts the conventional approximate $SU(6)$ spin-flavor symmetry, while entanglement suppression predicts a much larger $SU(16)$ symmetry under which the two spin states of the baryon octet transform as a 16-dimensional representation. To see this, consider the EFT in the $SU(3)$ flavor symmetry limit of QCD, where six independent contact operators contribute at LO [11],

$$\begin{aligned} \mathcal{L}_{\text{LO}}^{n_f=3} = & -c_1 \langle B_i^\dagger B_i B_j^\dagger B_j \rangle - c_2 \langle B_i^\dagger B_j B_j^\dagger B_i \rangle \\ & - c_3 \langle B_i^\dagger B_j^\dagger B_i B_j \rangle - c_4 \langle B_i^\dagger B_i^\dagger B_j B_j \rangle \\ & - c_5 \langle B_i^\dagger B_i \rangle \langle B_j^\dagger B_j \rangle - c_6 \langle B_i^\dagger B_j \rangle \langle B_j^\dagger B_i \rangle , \end{aligned} \quad (5)$$

where $\langle \dots \rangle$ denotes a trace in flavor space, and B_i is the

3×3 octet-baryon matrix where the subscript $i = 1, 2$ denotes spin. $\mathcal{L}_{\text{LO}}^{n_f=3}$ is invariant under rotations and the transformation $B \rightarrow VBV^\dagger$ where V is an $SU(3)$ matrix. In the large- N_c limit of QCD, an $SU(6)$ spin-flavor symmetry emerges relating the six coefficients c_i in Eq. (5) to two independent coefficients a, b [6] in the $SU(6)$ invariant Lagrange density,

$$\begin{aligned} c_1 = & -\frac{7}{27}b, \quad c_2 = \frac{1}{9}b, \quad c_3 = \frac{10}{81}b, \\ c_4 = & -\frac{14}{81}b, \quad c_5 = a + \frac{2}{9}b, \quad c_6 = -\frac{1}{9}b. \end{aligned} \quad (6)$$

A comprehensive set of lattice QCD calculations of light nuclei, hypernuclei and low-energy baryon-baryon scattering in the limit of $SU(3)$ flavor symmetry by the NPLQCD collaboration [19, 61, 62] demonstrates that the c_i are consistent with this predicted $SU(6)$ spin-flavor symmetry [19]. The two-baryon sector calculated with $m_\pi \sim 800$ MeV is found to be unnatural [19, 61, 62], with a scattering length that is larger than the range of the interaction, and hence better described by the power-counting of van Kolck [63] and KSW [58, 59, 64]. Further, the values of c_1, c_2, c_3, c_4 and c_6 are calculated to be much smaller than c_5 , indicating that $b \ll a$ [19, 61, 62]. When $b = 0$, the $SU(6)$ is enlarged to an emergent $SU(16)$ spin-flavor symmetry [19], where the baryon states populate the fundamental of $SU(16)$,

$$\mathcal{L}_{\text{LO}}^{n_f=3} \rightarrow -\frac{1}{2}c_S (\mathcal{B}^\dagger \mathcal{B})^2 \quad \mathcal{B} = (p_{\uparrow}, p_{\downarrow}, n_{\uparrow}, n_{\downarrow}, \Lambda_{\uparrow}, \dots)^T, \quad (7)$$

with $c_S = 2c_5$.

The existence of $SU(16)$ symmetry and $b = 0$ does not follow from the large- N_c expansion, but does follow from entanglement suppression. The entanglement power of the S -matrix in spin-space from the $n_f = 3$ interactions in Eq. (5) can be addressed by considering its action on states of distinguishable baryons. Computing the entanglement power $\mathcal{E}(\hat{\mathbf{S}})$ for more than six distinct two-baryon channels with nonidentical particles—e.g., ΛN , $\Xi^- p$ —shows that zero entanglement power occurs at the $SU(16)$ point where all the c_n couplings vanish except for c_5 , which is unconstrained (and all LO scattering matrices in the $J = 0$ and $J = 1$ mixed-flavor sectors are diagonal [11, 19]). Thus, the principle of entanglement suppression gives rise to an approximate symmetry, apparent in lattice QCD calculations [19, 61, 62], that does not follow from the large- N_c limit. We conclude that the large- N_c limit of QCD does not provide a sufficiently stringent constraint to produce a low-energy EFT that does not entangle, which could not be deduced from the $n_f = 2$ sector alone [6]. Thus, the entanglement power of the S -matrix appears to be a dominant ingredient in dictating the properties and relative size of interactions in low-energy nuclear and hypernuclear systems.

While in nuclei and hypernuclei contributions to binding from three-body forces between nucleons and hyperons are small compared with those from two-baryon

forces, they cannot be neglected and become more important with increasing density. To understand whether entanglement suppression dictates approximate $SU(16)$ symmetry in these interactions as well, we take a more general approach rather than computing the multibaryon S -matrix in various channels to constrain couplings. We begin by assuming exact $SU(2)_{\text{spin}} \times SU(3)_{\text{flavor}}$ symmetry, where corrections due to $SU(3)$ violation from quark mass differences can be incorporated in the usual way. Even in the degenerate quark mass limit, this means restricting ourselves to considering only interactions that do not couple spin to orbital angular momentum. While such spin-orbit and tensor interactions can be important in heavy nuclei, they are suppressed by powers of the baryon momenta and do not enter the IR limit of the effective theory. It is then argued that entanglement suppression requires the interactions to respect a $U(1)^{16}$ symmetry, conserving particle number individually for each of the octet baryon spin states. To see why this is a reasonable assumption, consider a 1-body operator (which need not be local) that violates the $U(1)^{16}$ symmetry, e.g.,

$$\hat{\Theta} = \int d^3v d^3u [f(v - u)\alpha_v^\dagger \beta_u + \text{h.c.}], \quad (8)$$

where α, β are annihilation operators for components of \mathcal{B} with $\alpha \neq \beta$, \mathbf{u} and \mathbf{v} are spatial coordinates and f is a form factor. This operator implements the transformation, e.g.,

$$\begin{aligned} \hat{\Theta}|\alpha_x, \beta_y, \gamma_z\rangle &= \int d^3w [f(w - y)|\alpha_x, \alpha_w, \gamma_z\rangle \\ &\quad + f^*(x - w)|\beta_w, \beta_y, \gamma_z\rangle], \end{aligned} \quad (9)$$

producing an entangled state, even if $f(\mathbf{x} - \mathbf{y}) = \delta^3(\mathbf{x} - \mathbf{y})$, from which it can be concluded that the $U(1)^{16}$ symmetry is a necessary condition to forbid entangling interactions³. It follows from simultaneous exact $SU(2) \times SU(3)$ and $U(1)^{16}$ symmetries that the LO EFT must respect the full $SU(16)$ symmetry by the following argument. The charges $Q_\alpha = \mathcal{B}^\dagger \Gamma_\alpha \mathcal{B}$ that by assumption commute with the Hamiltonian H consist of

$$\Gamma_\alpha \in \{\mathcal{I}_{16}, S_i \otimes \mathcal{I}_8, \mathcal{I}_2 \otimes t_a, M_i\} \quad , \quad (10)$$

where $S_{1,2,3} \in \mathfrak{su}(2)$ are the fundamental generators of $SU(2)$, $t_a \in \mathfrak{su}(3)$ with $(t_a)_{bc} = -if_{abc}$ for $a, b, c = 1, \dots, 8$ are the generators of the $SU(3)$ adjoint representation with structure constants f_{abc} , and the M_i for $i = 1, \dots, 15$ are a set of independent diagonal traceless 16×16 matrices generating $U(1)^{15}$, the ignored $U(1)$ symmetry being baryon number. Since all of the above Q^α are assumed

to commute with H , it follows that their commutators do as well. The full symmetry of H will be the symmetry group generated by the closure of the Q^α under commutation. By making use of the fact that the t_a generate an irreducible representation of the $\mathfrak{su}(3)$ Lie algebra and invoking Schur's Lemma, it is possible to show that this full symmetry algebra is $\mathfrak{su}(16)$ [52].

Conjecturing that the guiding principle for low-energy nuclear and hypernuclear forces is the suppression of entanglement fluctuations provides important theoretical constraints on dense matter systems. The Lagrange density describing the $n_f = 2$ sector with vanishing entanglement power, and therefore $SU(4)$ spin-flavor symmetry, is

$$\mathcal{L}^{(n_f=2)} = - \sum_{n=2}^4 \frac{1}{n!} C_S^{(n)} (N^\dagger N)^n \quad , \quad (11)$$

while for $n_f = 3$ with $SU(16)$ spin-flavor symmetry,

$$\mathcal{L}^{(n_f=3)} = - \sum_{n=2}^{16} \frac{1}{n!} c_S^{(n)} (\mathcal{B}^\dagger \mathcal{B})^n . \quad (12)$$

Calculations of hypernuclei and hyperon-nucleon interactions imposing $SU(16)$ spin-flavor symmetry on the low-energy forces are now in progress [65]. Our work suggests that such calculations could probe the nature of entanglement in strong interactions.

The Pauli exclusion principle's requirement of antisymmetrization produces a natural tendency for highly entangled states of identical particles in the s -channels. It is somewhat perplexing how to understand the result that the S -matrix for baryon-baryon scattering exhibits screening of entanglement power when the quarks and gluons that form the nucleon are highly entangled. It may be the case that the nonperturbative mechanisms of confinement and chiral symmetry breaking together strongly screen entanglement fluctuations in the low-energy sector of QCD beyond what can be identified in the large- N_c limit of QCD.

While our work has focused on low-energy interactions, preliminary evidence for entanglement suppression at higher orders in a derivative expansion is seen in the $n_f = 2$ low-energy constants (LECs) for operators up to NNLO. The contact terms of the two-nucleon potential in the center-of-mass frame are [66]

$$V_{\text{contact}} = C_S + C_T \vec{\sigma}_1 \cdot \vec{\sigma}_2 + V_{\text{contact}}^{(2)}, \quad (13)$$

$$V_{\text{contact}}^{(2)} = C_1 \vec{q}^2 + C_3 \vec{q}^2 (\vec{\sigma}_1 \cdot \vec{\sigma}_2) + C_6 (\vec{q} \cdot \vec{\sigma}_1)(\vec{q} \cdot \vec{\sigma}_2) ,$$

with $\vec{q} = \vec{p}' - \vec{p}$ and \vec{p}, \vec{p}' the initial and final nucleon momenta. Calculating their entanglement power, it is expected that C_T, C_3 , and C_6 will be suppressed at low energies. Numerical values of these potential coefficients are determined from the values of the spectroscopic LECs [67–69] (see Fig. 1 of the supplementary material). At small values of the maximum scattering

³ The converse is not true: it is possible to show that there exist entangling interactions which preserve $U(1)^{16}$ symmetry [52].

energy, T_{Lab}^{\max} , the coefficients of the non-entangling operators, C_S and C_1 , are found to be larger in magnitude than their entangling counterparts. Furthermore, as T_{Lab}^{\max} is increased and shorter distances scales are probed, the suppression lessens and C_6 grows. While these observations are consistent with entanglement-suppressed LECs, work remains to be done in understanding the mechanism that suppresses entanglement power in the transition from QCD to low-energy effective interactions, and the full consequences of this mechanism.

Nuclear physics, with its rich theoretical structure and phenomenology emerging from QCD and QED in the infrared, provides a unique forum for the study of fundamental properties of quantum entanglement. We conjecture that the suppression of entanglement is an important element of strong-interaction physics that is correlated with enhanced emergent symmetries.

We would like to thank A. Cervera-Lierta, D. Lonardoni, A. Muran, and A. Roggero for inspiring discussions and A. Ekström for providing additional details for the LEC correlations in Ref. [67]. SRB was supported in part by the U. S. Department of Energy grant DE-SC001347. DBK, NK and MJS were supported by DOE grant No. DE-FG02-00ER41132, and NK was supported in part by a Microsoft Research PhD Fellowship.

-
- [1] G. 't Hooft, *Nucl. Phys.* **B72**, 461 (1974), [,337(1973)].
[2] E. Witten, *Annals Phys.* **128**, 363 (1980).
[3] E. Wigner, *Phys. Rev.* **51**, 106 (1937).
[4] E. Wigner, *Phys. Rev.* **51**, 947 (1937).
[5] E. P. Wigner, *Phys. Rev.* **56**, 519 (1939).
[6] D. B. Kaplan and M. J. Savage, *Phys. Lett.* **B365**, 244 (1996), arXiv:hep-ph/9509371 [hep-ph].
[7] D. B. Kaplan and A. V. Manohar, *Phys. Rev.* **C56**, 76 (1997), arXiv:nucl-th/9612021 [nucl-th].
[8] A. Calle Cordon and E. Ruiz Arriola, *Phys. Rev.* **C78**, 054002 (2008), arXiv:0807.2918 [nucl-th].
[9] X. Liu, V. Limkaisang, D. Samart, and Y. Yan, (2017), arXiv:1710.10068 [hep-ph].
[10] M. R. Schindler, H. Singh, and R. P. Springer, *Phys. Rev.* **C98**, 044001 (2018), arXiv:1805.06056 [nucl-th].
[11] M. J. Savage and M. B. Wise, *Phys. Rev.* **D53**, 349 (1996), arXiv:hep-ph/9507288 [hep-ph].
[12] H. Polinder, J. Haidenbauer, and U.-G. Meissner, *Nucl. Phys.* **A779**, 244 (2006), arXiv:nucl-th/0605050 [nucl-th].
[13] D. R. Phillips and C. Schat, *Phys. Rev.* **C88**, 034002 (2013), arXiv:1307.6274 [nucl-th].
[14] E. Epelbaum, A. M. Gasparyan, H. Krebs, and C. Schat, *Eur. Phys. J.* **A51**, 26 (2015), arXiv:1411.3612 [nucl-th].
[15] J. Vanasse and D. R. Phillips, *Few Body Syst.* **58**, 26 (2017), arXiv:1607.08585 [nucl-th].
[16] D. R. Phillips, D. Samart, and C. Schat, *Phys. Rev. Lett.* **114**, 062301 (2015), arXiv:1410.1157 [nucl-th].
[17] M. R. Schindler, R. P. Springer, and J. Vanasse, *Phys. Rev.* **C93**, 025502 (2016), [Erratum: *Phys. Rev.* C97,no.5,059901(2018)], arXiv:1510.07598 [nucl-th].
[18] M. J. Savage, *Nucl. Phys.* **A695**, 365 (2001), arXiv:nucl-th/0012043 [nucl-th].
[19] M. L. Wagman, F. Winter, E. Chang, Z. Davoudi, W. Detmold, K. Orginos, M. J. Savage, and P. E. Shahan, *Phys. Rev.* **D96**, 114510 (2017), arXiv:1706.06550 [hep-lat].
[20] A. Cervera-Lierta, J. I. Latorre, J. Rojo, and L. Rottoli, *SciPost Phys.* **3**, 036 (2017), arXiv:1703.02989 [hep-th].
[21] A. Einstein, B. Podolsky, and N. Rosen, *Phys. Rev.* **47**, 777 (1935).
[22] J. S. Bell, *Physics Physique Fizika* **1**, 195 (1964).
[23] A. Aspect, P. Grangier, and G. Roger, *Phys. Rev. Lett.* **47**, 460 (1981).
[24] S. J. Freedman and J. F. Clauser, *Phys. Rev. Lett.* **28**, 938 (1972).
[25] S. Ryu and T. Takayanagi, *Phys. Rev. Lett.* **96**, 181602 (2006), arXiv:hep-th/0603001 [hep-th].
[26] S. Ryu and T. Takayanagi, *JHEP* **08**, 045 (2006), arXiv:hep-th/0605073 [hep-th].
[27] J. Maldacena and L. Susskind, *Fortsch. Phys.* **61**, 781 (2013), arXiv:1306.0533 [hep-th].
[28] P. V. Buividovich and M. I. Polikarpov, *Phys. Lett.* **B670**, 141 (2008), arXiv:0806.3376 [hep-th].
[29] P. V. Buividovich and M. I. Polikarpov, *Proceedings, 8th Conference on Quark Confinement and the Hadron Spectrum (Confinement8): Mainz, Germany, September 1-6, 2008, PoS CONFINEMENT8*, 039 (2008), [*J. Phys.A42,304005(2009)*], arXiv:0811.3824 [hep-lat].
[30] Y. Nakagawa, A. Nakamura, S. Motoki, and V. I. Zakharov, *Proceedings, 27th International Symposium on Lattice field theory (Lattice 2009): Beijing, P.R. China, July 26-31, 2009, PoS LAT2009*, 188 (2009), arXiv:0911.2596 [hep-lat].
[31] W. Donnelly, *Phys. Rev.* **D85**, 085004 (2012), arXiv:1109.0036 [hep-th].
[32] H. Casini, M. Huerta, and J. A. Rosabal, *Phys. Rev.* **D89**, 085012 (2014), arXiv:1312.1183 [hep-th].
[33] D. Radicevic, (2014), arXiv:1404.1391 [hep-th].
[34] S. Ghosh, R. M. Soni, and S. P. Trivedi, *Journal of High Energy Physics* **2015**, 69 (2015).
[35] E. Itou, K. Nagata, Y. Nakagawa, A. Nakamura, and V. I. Zakharov, *PTEP* **2016**, 061B01 (2016), arXiv:1512.01334 [hep-th].
[36] S. Aoki, T. Iritani, M. Nozaki, T. Numasawa, N. Shiba, and H. Tasaki, *Journal of High Energy Physics* **2015**, 187 (2015).
[37] R. M. Soni and S. P. Trivedi, *JHEP* **01**, 136 (2016), arXiv:1510.07455 [hep-th].
[38] K. Van Acoleyen, N. Bultinck, J. Haegeman, M. Marien, V. B. Scholz, and F. Verstraete, *Phys. Rev. Lett.* **117**, 131602 (2016).
[39] E. Witten, *Rev. Mod. Phys.* **90**, 045003 (2018), arXiv:1803.04993 [hep-th].
[40] T. C. Rogers and P. J. Mulders, *Phys. Rev.* **D81**, 094006 (2010), arXiv:1001.2977 [hep-ph].
[41] C. M. Ho and S. D. H. Hsu, *Mod. Phys. Lett.* **A31**, 1650110 (2016), arXiv:1506.03696 [hep-th].
[42] D. E. Kharzeev and E. M. Levin, *Phys. Rev.* **D95**, 114008 (2017), arXiv:1702.03489 [hep-ph].
[43] J. Berges, S. Floerchinger, and R. Venugopalan, *Phys. Lett.* **B778**, 442 (2018), arXiv:1707.05338 [hep-ph].
[44] E. Shuryak and I. Zahed, *Annals Phys.* **396**, 1 (2018),

- arXiv:1707.01885 [hep-ph].
- [45] O. K. Baker and D. E. Kharzeev, Phys. Rev. **D98**, 054007 (2018), arXiv:1712.04558 [hep-ph].
- [46] J. Berges, S. Floerchinger, and R. Venugopalan, JHEP **04**, 145 (2018), arXiv:1712.09362 [hep-th].
- [47] Y. Hagiwara, Y. Hatta, B.-W. Xiao, and F. Yuan, Phys. Rev. **D97**, 094029 (2018), arXiv:1801.00087 [hep-ph].
- [48] Y. Liu and I. Zahed, (2018), arXiv:1803.09157 [hep-ph].
- [49] A. Kovner, M. Lublinsky, and M. Serino, (2018), 10.1016/j.physletb.2018.10.043, arXiv:1806.01089 [hep-ph].
- [50] P. Zanardi, Phys. Rev. A **63**, 040304 (2001).
- [51] A. D. Ballard and Y.-S. Wu, “Cross disciplinary advances in quantum computing,” (American Mathematical Society, 2011) Chap. Cartan Decomposition and Entangleing Power of Braiding Quantum Gates.
- [52] S. R. Beane, D. B. Kaplan, N. Klco, and M. J. Savage, in preparation.
- [53] V. G. J. Stoks, R. A. M. Klomp, M. C. M. Rentmeester, and J. J. de Swart, Phys. Rev. C **48**, 792 (1993).
- [54] V. G. J. Stoks, R. A. M. Klomp, C. P. F. Terheggen, and J. J. de Swart, Phys. Rev. C **49**, 2950 (1994).
- [55] T. A. Rijken and V. G. J. Stoks, Phys. Rev. C **54**, 2851 (1996).
- [56] T. A. Rijken and V. G. J. Stoks, Phys. Rev. C **54**, 2869 (1996).
- [57] R. U. Nijmegen, “NN-Online,” <http://nn-online.org/> (2005), accessed: 2018-12-01.
- [58] D. B. Kaplan, M. J. Savage, and M. B. Wise, Phys. Lett. B **424**, 390 (1998), arXiv:nucl-th/9801034 [nucl-th].
- [59] D. B. Kaplan, M. J. Savage, and M. B. Wise, Nucl. Phys. B **534**, 329 (1998), arXiv:nucl-th/9802075 [nucl-th].
- [60] T. Mehen, I. W. Stewart, and M. B. Wise, Phys. Rev. Lett. **83**, 931 (1999), arXiv:hep-ph/9902370 [hep-ph].
- [61] S. R. Beane, E. Chang, S. D. Cohen, W. Detmold, H. W. Lin, T. C. Luu, K. Orginos, A. Parreno, M. J. Savage, and A. Walker-Loud (NPLQCD), Phys. Rev. **D87**, 034506 (2013), arXiv:1206.5219 [hep-lat].
- [62] S. R. Beane *et al.* (NPLQCD), Phys. Rev. **C88**, 024003 (2013), arXiv:1301.5790 [hep-lat].
- [63] U. van Kolck, Nucl. Phys. **A645**, 273 (1999), arXiv:nucl-th/9808007 [nucl-th].
- [64] J.-W. Chen, G. Rupak, and M. J. Savage, Nucl. Phys. **A653**, 386 (1999), arXiv:nucl-th/9902056 [nucl-th].
- [65] D. Lonardoni and A. Roggero, “Spin-flavor symmetries in hypernuclei and nuclei,” (2018), in preparation.
- [66] E. Epelbaum, W. Glockle, and U. G. Meissner, Nucl. Phys. **A747**, 362 (2005), arXiv:nucl-th/0405048 [nucl-th].
- [67] B. D. Carlsson, A. Ekstrom, C. Forssen, D. F. Stromberg, G. R. Jansen, O. Lilja, M. Lindby, B. A. Mattsson, and K. A. Wendt, Phys. Rev. **X6**, 011019 (2016), arXiv:1506.02466 [nucl-th].
- [68] E. Epelbaum, U. G. Meissner, W. Gloeckle, and C. Elster, Phys. Rev. **C65**, 044001 (2002), arXiv:nucl-th/0106007 [nucl-th].
- [69] E. Epelbaum, H. Krebs, and U. G. Meissner, Eur. Phys. J. **A51**, 53 (2015), arXiv:1412.0142 [nucl-th].

Supplemental Material for “Entanglement Suppression and Emergent Symmetries of Strong Interactions”

In this supplemental material, Fig. 3 shows the scaling of low energy constants (LECs) relevant for the two-nucleon potential in the center-of-mass frame. The data in Fig. 3 have been compiled from the spectroscopic LECs and associated correlated uncertainties that were fit in Ref. [67]. With the inclusion of experimental data up to a maximum scattering energy T_{Lab}^{\max} , the stability of the potential coefficients suggests that the LECs are well-constrained by low-energy data well-below pion threshold. The progression from solid to dashed to dotted lines in Fig. 3 shows the shift in these coefficients with increasing regulator-energy cutoffs of $\Lambda = 450, 475, 550, 600$ MeV. Numerical values of the data shown in Fig. 3 may be found in Table I while that of Fig. 1 of the main text may be found in Table II.

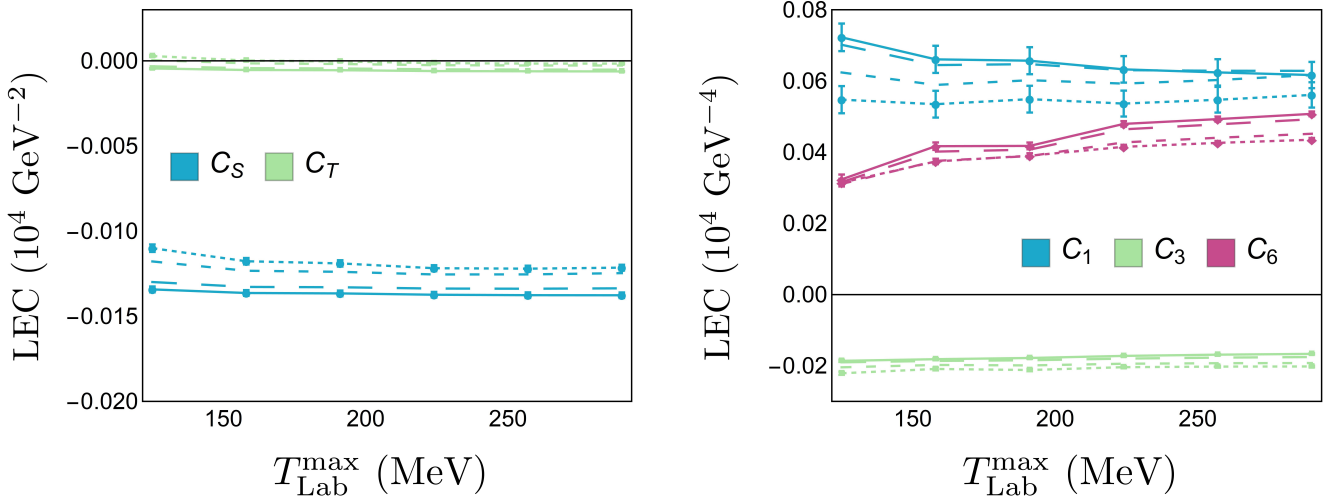


FIG. 3. Low-energy constants of the NNLO two-nucleon interaction at $\mathcal{O}(p^0)$ (left panel) and $\mathcal{O}(p^2)$ (right panel) as a function of the maximum scattering energy retained in the fitted experimental data set, T_{Lab}^{\max} , determined from NN and πN scattering [67]. The value of the regulator cutoff corresponds to $\Lambda = 450$ MeV for the solid line, $\Lambda = 475$ MeV for the long-dashed line, $\Lambda = 550$ MeV for the dashed line and $\Lambda = 600$ MeV for the dotted line. The uncertainties on the solid and dotted lines are propagated from the correlated uncertainties of the spectroscopic LECs fit in Ref. [67].

$\Lambda = 450$	$T_{\text{Lab}}^{\max} = 125$	$T_{\text{Lab}}^{\max} = 158$	$T_{\text{Lab}}^{\max} = 191$	$T_{\text{Lab}}^{\max} = 224$	$T_{\text{Lab}}^{\max} = 257$	$T_{\text{Lab}}^{\max} = 290$
C_S	-0.01342(17)	-0.01363(17)	-0.01366(17)	-0.01374(17)	-0.01376(17)	-0.01377(16)
C_T	-0.00045(2)	-0.00053(2)	-0.00055(2)	-0.00060(2)	-0.00061(1)	-0.00062(1)
C_1	0.0723(39)	0.0661(38)	0.0657(38)	0.0633(37)	0.0624(37)	0.0617(37)
C_3	-0.0186(3)	-0.0181(3)	-0.0178(2)	-0.0172(2)	-0.0169(2)	-0.0167(2)
C_6	0.0324(14)	0.0417(10)	0.0418(9)	0.0480(8)	0.0493(7)	0.0508(7)
$\Lambda = 475$	$T_{\text{Lab}}^{\max} = 125$	$T_{\text{Lab}}^{\max} = 158$	$T_{\text{Lab}}^{\max} = 191$	$T_{\text{Lab}}^{\max} = 224$	$T_{\text{Lab}}^{\max} = 257$	$T_{\text{Lab}}^{\max} = 290$
C_S	-0.01299(18)	-0.01328(17)	-0.01330(17)	-0.01337(17)	-0.01338(17)	-0.01336(16)
C_T	-0.00032(2)	-0.00043(2)	-0.00045(2)	-0.00050(2)	-0.00051(2)	-0.00052(2)
C_1	0.0702(39)	0.0645(38)	0.0647(38)	0.0630(37)	0.0629(37)	0.0629(37)
C_3	-0.0190(3)	-0.0186(3)	-0.0184(2)	-0.0180(2)	-0.0177(2)	-0.0175(2)
C_6	0.0316(13)	0.0402(10)	0.0407(9)	0.0464(7)	0.0478(7)	0.0493(6)
$\Lambda = 550$	$T_{\text{Lab}}^{\max} = 125$	$T_{\text{Lab}}^{\max} = 158$	$T_{\text{Lab}}^{\max} = 191$	$T_{\text{Lab}}^{\max} = 224$	$T_{\text{Lab}}^{\max} = 257$	$T_{\text{Lab}}^{\max} = 290$
C_S	-0.01178(19)	-0.01233(18)	-0.01239(18)	-0.01254(17)	-0.01254(17)	-0.01247(17)
C_T	0.00004(4)	-0.00014(3)	-0.00018(3)	-0.00025(2)	-0.00027(2)	-0.00027(2)
C_1	0.0624(38)	0.0589(38)	0.0602(37)	0.0593(37)	0.0603(36)	0.0617(36)
C_3	-0.0204(4)	-0.0198(3)	-0.0199(3)	-0.0194(2)	-0.0193(2)	-0.0192(2)
C_6	0.0311(11)	0.0376(8)	0.0389(7)	0.0428(6)	0.0441(6)	0.0452(5)
$\Lambda = 600$	$T_{\text{Lab}}^{\max} = 125$	$T_{\text{Lab}}^{\max} = 158$	$T_{\text{Lab}}^{\max} = 191$	$T_{\text{Lab}}^{\max} = 224$	$T_{\text{Lab}}^{\max} = 257$	$T_{\text{Lab}}^{\max} = 290$
C_S	-0.01100(22)	-0.01177(19)	-0.01189(19)	-0.01218(18)	-0.01220(17)	-0.01214(17)
C_T	0.00028(5)	0.00002(3)	-0.00003(3)	-0.00013(3)	-0.00016(3)	-0.00016(2)

C_1	0.0548(38)	0.0535(38)	0.0549(38)	0.0537(36)	0.0547(36)	0.0561(36)
C_3	-0.0221(4)	-0.0209(4)	-0.0212(3)	-0.0204(3)	-0.0202(3)	-0.0202(2)
C_6	0.0315(11)	0.0374(8)	0.0390(7)	0.0415(6)	0.0426(5)	0.0435(5)

TABLE I: Numerical values of the data shown in Fig. 3. Both Λ and T_{Lab}^{\max} are given in MeV. The values of $C_{S,T}$ and C_i are given in units of 10^4 GeV^{-2} and 10^4 GeV^{-4} , respectively. Central values and correlated uncertainties are calculated from the spectroscopic LECs fit to NN and πN scattering data given in Ref. [67].

While the main text has shown that the S -matrix entanglement power may be written as a simple function of the difference between the 1S_0 and 3S_1 phase shifts, it is enlightening to express the entanglement power directly in terms of lagrangian coefficients. In the context of the NN pionless EFT [58, 59, 63, 64], the nucleon-nucleon scattering amplitude (not including 3S_1 - 3D_1 mixing) may be determined in the PDS scheme [58, 59] as

$$i\mathcal{A} = \frac{-iC(p^2, \mu)}{1 + MC(p^2, \mu)(\mu + ip)/4\pi} , \quad (14)$$

furnishing a unitary S -matrix,

$$S = 1 + i \left(\frac{pM}{2\pi} \right) \mathcal{A} , \quad (15)$$

where M is the nucleon mass, μ is the renormalization scale, p is the magnitude of the center-of-mass nucleon momentum, and $C(p^2, \mu)$ is the tree-level s-wave vertex from the NN contact interactions. To analyze the production of entanglement in the spin sector, this vertex in the 1S_0 - 3S_1 channels is decomposed as

$$C(p^2, \mu)_\sigma = C_S \hat{\mathbf{1}} + C_T \hat{\boldsymbol{\sigma}} \cdot \hat{\boldsymbol{\sigma}} . \quad (16)$$

The relation between the μ -dependent coefficients and the phase shifts is

$$p \cot \delta_r = - \left(\frac{4\pi}{M \bar{C}_r} + \mu \right) , \quad (17)$$

for $r = 0, 1$ where δ_0, δ_1 are the scattering phase shifts in the 1S_0 and 3S_1 channels and spectroscopic coefficients are related to those in the vertex as

$$\bar{C}_0 = (C_S - 3C_T) \quad \bar{C}_1 = (C_S + C_T) . \quad (18)$$

These relations lead from the lagrangian interactions to the S -matrix structure of Eq. (3) of the main text and may be expressed here as

$$\hat{\mathbf{S}} = \left[1 - \frac{Mp}{2} \left[\frac{3\bar{C}_1}{D_1^-} + \frac{\bar{C}_0}{D_0^-} \right] \right] \hat{\mathbf{1}} + \frac{8i\pi C_T M p}{D_0^- D_1^-} \hat{\boldsymbol{\sigma}} \cdot \hat{\boldsymbol{\sigma}} , \quad D_j^\pm = M \bar{C}_j (p \pm i\mu) \pm 4i\pi . \quad (19)$$

The entanglement power of the S -matrix becomes

$$\mathcal{E}(\hat{\mathbf{S}}) = \frac{512\pi^2 C_T^2 M^2 p^2 (8\pi M \mu (C_S - C_T) + M^2 (p^2 + \mu^2) \bar{C}_1 \bar{C}_0 + 16\pi^2)^2}{3(D_0^-)^2 (D_1^-)^2 (D_0^+)^2 (D_1^+)^2} . \quad (20)$$

The curve of Fig. 4 shows this entanglement power as a function of the $\hat{\boldsymbol{\sigma}} \cdot \hat{\boldsymbol{\sigma}}$ interaction coefficient, C_T , focusing on the leading interaction in the effective lagrangian with the following numerical values: $C_S = -1.2 \times 10^{-4} \text{ MeV}^{-2}$, $\mu = 140 \text{ MeV}$, $M = 939 \text{ MeV}$ and $p = 19.4 \text{ MeV}$. The following scattering parameters have been used to calculate physical values of C_S and C_T : $a_0 = -23.714(13) \text{ fm}$, $a_1 = 5.425(1) \text{ fm}$, $r_0 = 2.73(3) \text{ fm}$, and $r_1 = 1.749(8) \text{ fm}$, where a and r are the scattering length and effective range, respectively.

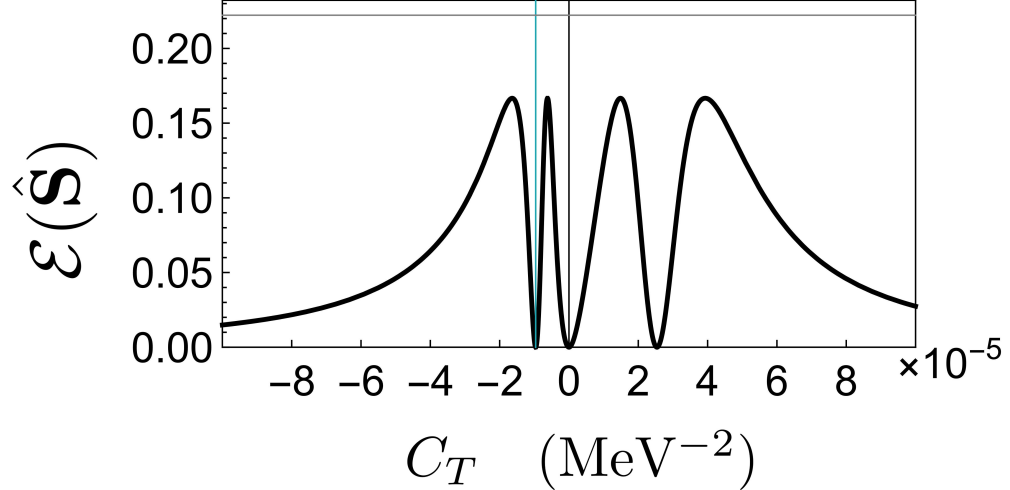


FIG. 4. Entanglement power of the S -matrix, $\mathcal{E}(\hat{\mathbf{S}})$, as a function of C_T evaluated with $C_S = -1.2 \times 10^{-4}$ MeV $^{-2}$, $\mu = 140$ MeV, $M = 939$ MeV, and $p = 19.4$ MeV. The vertical solid blue band indicates the physical value of $C_T = -9.605(3) \times 10^{-6}$ MeV $^{-2}$. The horizontal line at $\mathcal{E}(\hat{\mathbf{S}}) = \frac{2}{9}$ indicates the maximum two-body entanglement power of an unconstrained operator in SU(4).

p	$\mathcal{E}(\hat{\mathbf{S}})_{\text{pwa93}}$ [53]	$\mathcal{E}(\hat{\mathbf{S}})_{\text{esc96}}$ [55, 56]	$\mathcal{E}(\hat{\mathbf{S}})_{\text{nijm1}}$ [54]	$\mathcal{E}(\hat{\mathbf{S}})_{\text{reid93}}$ [54]
0.0000	9.9984×10^{-33}	9.9984×10^{-33}	9.9984×10^{-33}	9.9984×10^{-33}
0.6852	0.0067	0.0067	0.0003	0.0003
1.1868	0.0255	0.0255	0.0031	0.0031
1.5322	0.0312	0.0312	0.0083	0.0083
1.9380	0.0446	0.0446	0.0204	0.0204
2.2726	0.0635	0.0635	0.0363	0.0363
2.6538	0.0837	0.0837	0.0604	0.0604
2.9867	0.0977	0.0977	0.0845	0.0845
3.3568	0.1101	0.1101	0.1100	0.1101
3.6899	0.1209	0.1209	0.1284	0.1285
3.9954	0.1311	0.1311	0.1407	0.1407
4.3336	0.1419	0.1419	0.1497	0.1498
4.6473	0.1506	0.1506	0.1551	0.1551
4.9883	0.1578	0.1578	0.1591	0.1591
5.3075	0.1624	0.1624	0.1622	0.1622
5.6086	0.1651	0.1651	0.1648	0.1648
5.9340	0.1665	0.1665	0.1665	0.1665
6.2425	0.1665	0.1665	0.1665	0.1665
6.5722	0.1653	0.1653	0.1653	0.1653
6.8862	0.1629	0.1629	0.1629	0.1629
7.1864	0.1597	0.1597	0.1596	0.1597
7.5060	0.1554	0.1554	0.1553	0.1554
7.8125	0.1506	0.1506	0.1504	0.1505
8.3920	0.1402	0.1402	0.1398	0.1399
8.9339	0.1292	0.1292	0.1288	0.1290
9.4448	0.1182	0.1182	0.1180	0.1182
9.9295	0.1075	0.1075	0.1075	0.1078
10.3916	0.0973	0.0974	0.0974	0.0977
10.3916	0.0973	0.0974	0.0974	0.0977
11.2590	0.0789	0.0790	0.0790	0.0793
12.0642	0.0632	0.0633	0.0631	0.0635
13.0008	0.0469	0.0470	0.0468	0.0473
13.8743	0.0340	0.0341	0.0339	0.0344
14.6959	0.0239	0.0240	0.0238	0.0243

15.6250	0.0149	0.0149	0.0148	0.0152
16.5018	0.0085	0.0085	0.0084	0.0087
17.3344	0.0042	0.0042	0.0041	0.0044
18.2577	0.0012	0.0013	0.0012	0.0014
19.1366	0.0001	0.0001	0.0001	0.0001
19.9769	0.0002	0.0002	0.0003	0.0002
20.7832	0.0014	0.0014	0.0015	0.0013
21.6679	0.0038	0.0037	0.0038	0.0035
22.5180	0.0068	0.0067	0.0069	0.0065
23.3371	0.0105	0.0103	0.0106	0.0100
24.2255	0.0150	0.0148	0.0152	0.0144
25.0825	0.0199	0.0197	0.0201	0.0192
25.9111	0.0250	0.0248	0.0252	0.0242
26.7140	0.0302	0.0299	0.0304	0.0293
27.5788	0.0361	0.0357	0.0363	0.0350
28.4172	0.0419	0.0415	0.0421	0.0408
29.2317	0.0476	0.0472	0.0479	0.0464
33.5678	0.0779	0.0773	0.0782	0.0763
36.8992	0.0991	0.0983	0.0995	0.0974
39.9537	0.1160	0.1152	0.1164	0.1143
42.7908	0.1292	0.1284	0.1296	0.1276
45.4511	0.1395	0.1388	0.1399	0.1380
47.9640	0.1475	0.1467	0.1478	0.1461
50.3518	0.1535	0.1528	0.1538	0.1523
52.6313	0.1580	0.1574	0.1583	0.1570
54.8161	0.1614	0.1608	0.1616	0.1605
56.9170	0.1637	0.1633	0.1639	0.1630
58.9432	0.1653	0.1650	0.1654	0.1648
60.9020	0.1662	0.1660	0.1663	0.1659
62.7997	0.1666	0.1665	0.1666	0.1665
64.6417	0.1666	0.1667	0.1666	0.1667
66.4327	0.1663	0.1665	0.1662	0.1665
68.1766	0.1657	0.1660	0.1656	0.1661
69.8770	0.1649	0.1653	0.1647	0.1654
71.5371	0.1639	0.1644	0.1637	0.1646
73.1594	0.1628	0.1634	0.1625	0.1636
74.7466	0.1615	0.1623	0.1612	0.1625
76.3007	0.1602	0.1611	0.1599	0.1613
77.8238	0.1588	0.1598	0.1584	0.1600
89.0761	0.1465	0.1485	0.1459	0.1484
100.2362	0.1331	0.1360	0.1323	0.1355
110.2726	0.1214	0.1251	0.1205	0.1239
120.4473	0.1104	0.1149	0.1094	0.1129
130.7280	0.1002	0.1055	0.0993	0.1027
141.0915	0.0911	0.0972	0.0902	0.0935
151.5208	0.0830	0.0899	0.0821	0.0852
162.0032	0.0757	0.0834	0.0750	0.0778
172.5291	0.0692	0.0778	0.0687	0.0712
183.0910	0.0635	0.0729	0.0632	0.0654
193.6829	0.0584	0.0686	0.0583	0.0603
203.7248	0.0541	0.0651	0.0543	0.0561
213.8441	0.0502	0.0620	0.0506	0.0524
224.0302	0.0466	0.0593	0.0474	0.0491
234.2745	0.0435	0.0569	0.0445	0.0462
244.5696	0.0406	0.0549	0.0419	0.0436
254.9094	0.0380	0.0531	0.0395	0.0414
265.2886	0.0357	0.0516	0.0374	0.0395
275.7028	0.0336	0.0503	0.0356	0.0378
285.7377	0.0318	0.0493	0.0340	0.0365
295.8290	0.0302	0.0484	0.0325	0.0353
305.9711	0.0288	0.0476	0.0312	0.0343
316.1591	0.0276	0.0470	0.0300	0.0334
326.3886	0.0265	0.0466	0.0289	0.0327
336.6561	0.0256	0.0462	0.0280	0.0321

346.9579	0.0248	0.0460	0.0271	0.0316
356.9626	0.0243	0.0458	0.0264	0.0312
367.0144	0.0239	0.0458	0.0257	0.0310
377.1095	0.0236	0.0458	0.0250	0.0307
387.2445	0.0235	0.0459	0.0245	0.0306

TABLE II: Entanglement power, $\mathcal{E}(\hat{\mathbf{S}})$, of the S -matrix as a function of p , the center-of-mass nucleon momentum. This data is graphically shown in Fig. 1 of the main text. The 1S_0 and 3S_1 phase shifts used to calculate $\mathcal{E}(\hat{\mathbf{S}})$ were determined by four different models accessed through the NN-Online database [57].